



Cerebrovascular endothelial cells form transient Notch-dependent cystic structures in zebrafish

Elisabeth C Kugler^{1,2,*} , Max van Lessen³, Stephan Daetwyler^{4,5}, Karishma Chhabria^{1,2}, Aaron M Savage^{1,2}, Vishmi Silva^{1,2}, Karen Plant^{1,2}, Ryan B MacDonald^{1,2}, Jan Huisken^{4,6}, Robert N Wilkinson^{1,2}, Stefan Schulte-Merker³, Paul Armitage^{1,†} & Timothy JA Chico^{1,2,**,†} 

Abstract

We identify a novel endothelial membrane behaviour in transgenic zebrafish. Cerebral blood vessels extrude large transient spherical structures that persist for an average of 23 min before regressing into the parent vessel. We term these structures “*kugeln*”, after the German for sphere. *Kugeln* are only observed arising from the cerebral vessels and are present as late as 28 days post fertilization. *Kugeln* do not communicate with the vessel lumen and can form in the absence of blood flow. They contain little or no cytoplasm, but the majority are highly positive for nitric oxide reactivity. *Kugeln* do not interact with brain lymphatic endothelial cells (BLECs) and can form in their absence, nor do they perform a scavenging role or interact with macrophages. Inhibition of actin polymerization, Myosin II, or Notch signalling reduces *kugel* formation, while inhibition of VEGF or Wnt dysregulation (either inhibition or activation) increases *kugel* formation. *Kugeln* represent a novel Notch-dependent NO-containing endothelial organelle restricted to the cerebral vessels, of currently unknown function.

Keywords angiogenesis; endothelial cell; Notch; VEGF; Wnt; zebrafish

Subject Categories Development & Differentiation; Vascular Biology & Angiogenesis

DOI 10.15252/embr.201847047 | Received 12 September 2018 | Revised 7 May 2019 | Accepted 10 May 2019 | Published online 18 June 2019

EMBO Reports (2019) 20: e47047

Introduction

Formation of mature blood vessels requires a wide range of endothelial behaviours. These include proliferation, migration, anastomosis, lumen formation, remodelling and pruning, alongside recruitment of non-endothelial cell types such as pericytes and

vascular smooth muscle cells [1–4]. Many of these processes can be studied *in vitro*, but *in vivo* models of vascular development allow observation of endothelial behaviour within a multicellular and complex physiological environment.

Because visualizing real-time embryonic vascular development in mammals is technically challenging, the zebrafish has become a widely applied model of vertebrate vascular development. Their translucency enables detailed observation of cellular behaviour without invasive instrumentation *in vivo* [5,6]. An increasing array of transgenic reporter lines that drive fluorescent gene expression in vascular cells is available. Coupling these with state-of-the-art imaging techniques, such as light sheet fluorescence microscopy (LSFM), enables detailed cellular and subcellular imaging for hours or even days during embryonic development [7,8]. This ability to observe vascular development in more detail and for longer durations provides new insights into blood vessel formation.

Endothelial and other cells are known to form a variety of membranous vesicles [9]. These include apoptotic bodies (1–4 µm diameter), microvesicles (0.15–1 µm diameter) and exosomes (40–150 nm diameter) [10]. There is increasing evidence that such vesicles play important roles in intracellular signalling [11] and in vascular diseases such as atherosclerosis [12]. Understanding the roles of such vesicles is therefore of both biological and clinical significance.

Here, we report a novel type of endothelial cell vesicle formation with characteristics that are entirely distinct from any previously described membrane behaviour. We show that endothelial cells (ECs) of the zebrafish cerebral vasculature (but not other vessels) extrude spherical structures far larger than any previously described microvesicle [10], and unlike previously described vesicles never detach from the parent endothelial cell.

Due to their unknown nature and function, we termed these structures *kugeln* (German for spheres) and we here characterize their morphology, dynamics, and sites of occurrence. We find that

1 Department of Infection, Immunity and Cardiovascular Disease, Medical School, University of Sheffield, Sheffield, UK

2 The Bateson Centre, Firth Court, University of Sheffield, Sheffield, UK

3 WWU Münster, Faculty of Medicine, Institute for Cardiovascular Organogenesis and Regeneration, Münster, Germany

4 Max Planck Institute of Molecular Cell Biology and Genetics, Dresden, Germany

5 Department of Cell Biology, The University of Texas Southwestern, Texas, TX, USA

6 Morgridge Institute for Research, Madison, WI, USA

*Corresponding author. Tel: +44 1142 2210 81; E-mail: ekugler1@sheffield.ac.uk

**Corresponding author. Tel: +44 1142 2223 96; E-mail: tj.chico@sheffield.ac.uk

†These authors contributed equally to this work as senior authors

kugeln are membranous protrusions that do not contain either nuclei or cytoplasm. Although very different in size and behaviour to other vesicular structures, inhibition of the cytoskeletal components filamentous actin (F-actin) formation or Myosin II reduced *kugeln* formation, as previously shown for cellular blebs [13]. *Kugeln* do not interact with brain lymphatic endothelial cells (BLECs) [14,15] or macrophages, nor do they serve as scavengers. *Kugeln* formation is not influenced by either increased membrane rigidity, nor osmotic pressure, which are known to impact platelet ballooning and cellular blebbing [13,16].

Kugel formation can proceed in the absence of blood flow. Furthermore, we show that central orchestrators of vascular development such as Notch, VEGF and Wnt signalling [17–20] all influence *kugel* formation.

Together, our data suggest that *kugeln* represent a previously undescribed EC membrane behaviour restricted to the cerebral vessels. Their function remains unknown, but their existence emphasizes that our understanding of the intricate processes during vascular development is far from complete.

Results

Endothelial cells of zebrafish cerebral vessels frequently develop large extruding spherical structures

We initially observed that the endothelial cells of the cerebral vessels of transgenic *Tg(kdrl:HRAS-mCherry)⁵⁹¹⁶* zebrafish expressing an endothelial membrane-tagged reporter protein [21] displayed rounded protrusions (Fig 1A). Although the appearance of these on single z-slices was similar to cross-sections of lumenized vessels, three-dimensional reconstruction showed them to be spherical ablu-minal protrusions (Movie EV1). Due to their shape and unknown nature, we termed these structures *kugeln*, after the German for sphere (singular *kugel*). The mean diameter of *kugeln* was $10.1 \pm 0.5 \mu\text{m}$ (s.e.m.) at 3 dpf (Fig 1B) exceeding the size of previously described membrane-derived vesicles [10].

Mean number of *kugeln* per embryo was 5.55 ± 1.12 (s.e.m.) at 3 dpf and was not significantly different between 3 and 5 dpf ($P = 0.8571$; Fig 1C). We were able to observe *kugeln* in 28 dpf animals (Fig 1D), confirming that *kugeln* are present beyond embryonic stages.

To exclude the possibility that *kugeln* arise as a strain-specific feature of the transgenic line *Tg(kdrl:HRAS-mCherry)⁵⁹¹⁶*, we imaged a different transgenic *Tg(fli1aep:CAAX-eGFP)* [22], which utilizes the pan-endothelial promoter *fli1a* [8] and prenylation to target eGFP to the endothelial membrane. Again, *kugeln* were observed to arise from cerebral vessels (Fig 1E). We furthermore induced transient expression of the plasmid pTol2-*fli1a:myr-mCherry* [23,24], which uses the same *fli1a* promoter, and utilizes myristoylation to label the EC membrane. This was performed in *Tg(gata1:dsRed)* transgenics to enable vessel localization. Again, *kugeln* were observed in these embryos (Fig 1F), demonstrating that *kugel* formation was independent of the transgenic construct used, the promoter driving its expression and the method of membrane tagging. Therefore, we concluded that *kugeln* represent a physiological behaviour of the EC membrane of the cranial vasculature.

We mapped the location of *kugeln* on parent vessels to determine their distribution. > 90% of *kugeln* arose from the central vessels of the cerebral vasculature (Fig 1G) and none from the trunk vasculature (aorta, intersegmental vessels, dorsal longitudinal anastomotic vessel or caudal vein) at the examined time-points. The specific vessels giving rise to *kugeln* are shown in Fig 1H.

Although individual *kugeln* were often unilateral (present left-side but not right-sided vessels, or vice versa), overall left/right distribution was not significantly different (Fig 1H).

Kugeln are highly dynamic transient structures

We next observed *kugel* behaviour over time. Time-lapse imaging revealed *kugeln* were both transient and highly dynamic (Fig 2A). Although we expected *kugeln* to form new vessels, interact with other ECs to anastomose or detach from parent vessels, *kugeln* always either regressed back into the parent vessel or persisted to the end of imaging without separation or anastomosis.

Quantification of *kugel* lifespan showed that while some regressed after minutes, others persisted for hours (Fig 2B). Further examination showed that *kugeln* displayed dynamic alteration in shape and size, including shape changes, enlargement and retraction (Fig 2C; Movie EV2). This dynamic behaviour was observed not only in *Tg(kdrl:HRAS-mCherry)⁵⁹¹⁶* animals but also in *Tg(fli1ep:CAAX-eGFP)* (Fig EV1A and B) and *Tg(fli1a:myr-mCherry)*, *Tg(gata1:dsRed)* (Fig EV1C).

Figure 1. Endothelial cells of the zebrafish embryonic cerebral vessels develop “*kugeln*”; large spherical membrane protrusions.

- A MIP of cerebral vessels of 3 dpf *Tg(kdrl:HRAS-mCherry)⁵⁹¹⁶* embryo (grey LUT; inverted). Higher magnification panel showing two *kugeln* (arrowheads) arising from the middle mesencephalic central artery (MMCTA).
- B Diameter of *kugeln* at 3 dpf (mean \pm s.e.m. 10.13 ± 0.49 ; $n = 93$ *kugeln* from 32 3 dpf embryos; three experimental repeats).
- C Number of *kugeln* per embryo in 3, 4 and 5 dpf animals was not statistically significantly different (mean \pm s.e.m. 3 dpf 5.47 ± 1.09 , 4 dpf 7.47 ± 1.46 , 5 dpf 7.09 ± 1.55 ; $P = 0.8571$; 3 dpf: 175 *kugeln* from 32 embryos; 4 dpf: 239 *kugeln* from 32 embryos; 5 dpf: 227 *kugeln* from 32 embryos; four experimental repeats; Kruskal–Wallis test).
- D *Kugeln* (arrowheads) could be observed in 28 dpf animals.
- E MIP of cerebral vessels of 4 dpf *Tg(fli1aep:CAAX-eGFP)* embryo (grey LUT; inverted). Higher magnification panel shows a *kugel* (arrowhead) protruding from the posterior mesencephalic central artery (PMCTA).
- F Single Z-plane micrograph of cerebral vessels of a 3 dpf *Tg(gata1:dsRed)*, injected with a *Tol2-fli1a:myr-Cherry* construct showing two *kugeln* (arrowheads) in the higher magnification panel protruding from the MMCTA.
- G Locations and proportion of *kugeln* on cerebral vessels (colour coded by vessel; total $n = 107$ *kugeln* from 34 4 dpf embryos; three experimental repeats). AMCTA— anterior mesencephalic central artery, BCA—basal communicating artery, CaDI—caudal division of internal carotid artery, CMV—communicating vessel, CTA—central arteries, MMCTA—middle mesencephalic central artery, MtA—metencephalic artery, PCS—posterior communicating segment, PMBC—posterior midbrain channel, PMCTA—posterior mesencephalic central artery, PRA—prosencephalic artery.
- H Location of *kugeln* by vessel and laterality (107 *kugeln* from 34 4 dpf embryos; three experimental repeats comparison of left vs right $P = 0.3592$; Mann–Whitney U-test).

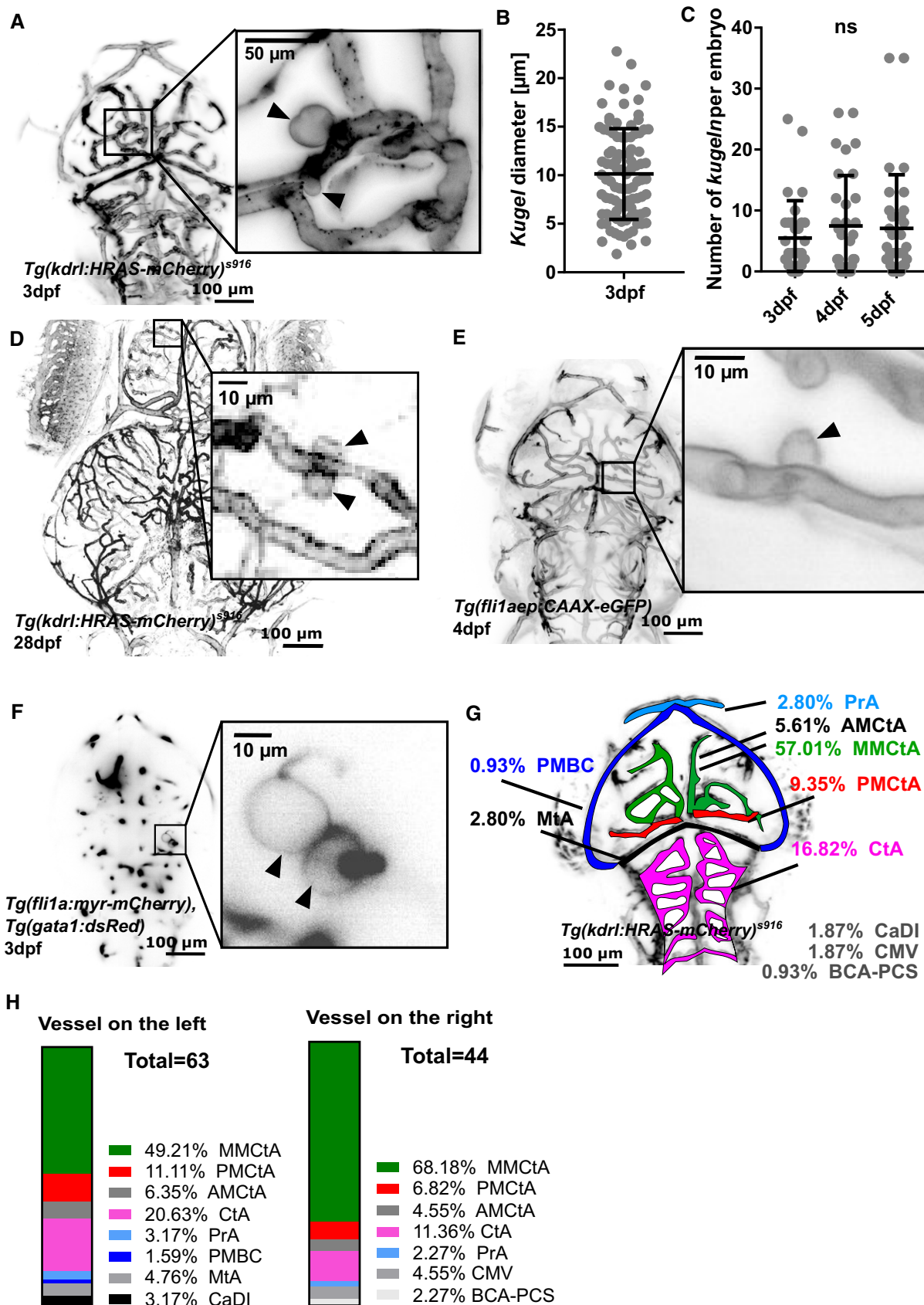


Figure 1.

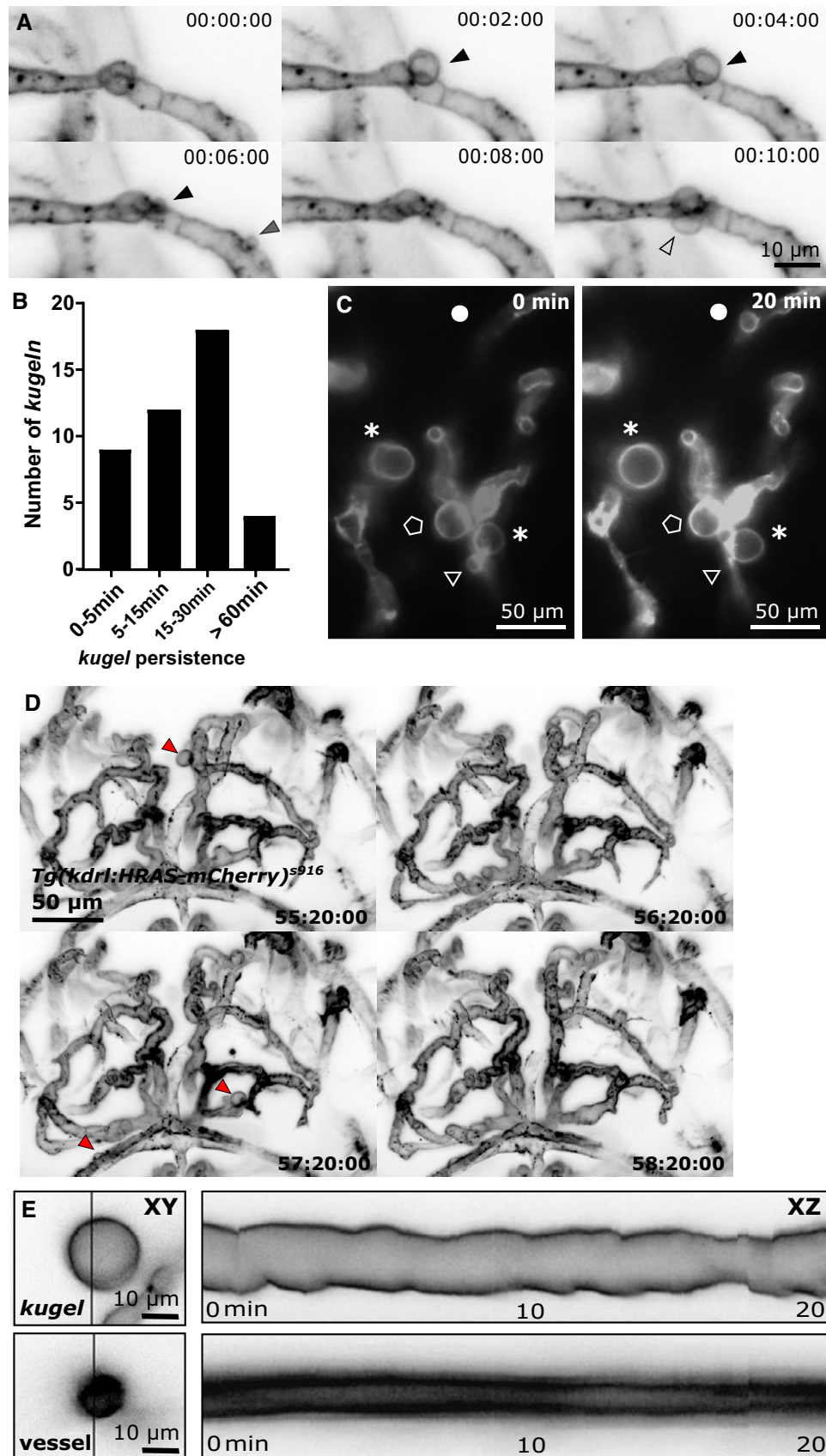


Figure 2.

Figure 2. Endothelial *kugel*n are transient and dynamically alter shape and size.

- A MIPs of a time-series light sheet acquisition shows three different *kugel*n (*kugel* 1—black arrowhead; *kugel* 2—grey arrowhead; *kugel* 3—unfilled arrowhead) protruding and retracting from parent vessels (2 min intervals; inverted LUT).
- B *Kugel*n persisted for variable durations before regression into the parent vessel (43 *kugel*n from 9 4 dpf embryos; four experimental repeats).
- C MIPs taken 20 min apart showing examples of different *kugel* behaviour including shape changes (asterisk), expansion (circle), retraction (triangle) or little change (pentagon).
- D MIPs taken 1 h apart show that *kugel*n may be observed at one time-point (red arrowhead, 55:20:00) but not 1 h later in the same animal (56:20:00) and to develop on other vessels 1 h later (57:20:00) which again have regressed by 58:20:00.
- E Kymographs generated by line-scanning across the diameter of a typical *kugel* shows that *kugel* diameter oscillated with a periodicity of minutes, while no such oscillations were observed in adjacent similarly sized cerebral vessels (all images grey LUT; inverted).

Although some animals displayed no *kugel*n when observed at a single time-point (Fig 1C), time-lapse imaging showed *kugel*n could develop at subsequent time-points (Fig 2D).

When we studied *kugel* shape change over time, this revealed that some *kugel*n displayed oscillatory diameter changes with a periodicity of minutes (Fig 2E). No such changes were observed in parent vessels, suggesting alterations of *kugel* size or shape are not directly related to blood pressure or flow but related to active membrane remodelling.

***Kugel*n are membranous structures whose formation is dependent on the cytoskeleton**

We next investigated the composition and biogenesis of *kugel*n. Examining double-transgenic embryos *Tg(kdr:nls-eGFP)^{zfl109}*, *Tg(kdrl:HRAS-mCherry)^{s916}* that labelled endothelial nuclei and membrane, we never observed *kugel*n to contain a nucleus, nuclear defragmentation or observed nuclear mitosis nearby *kugel*n (Fig 3A). This suggests *kugel*n do not represent an atypical form of cell proliferation, apoptosis or angiogenic sprouting.

Analysing the double-transgenic line *Tg(fli1a:LifeAct-mClover)^{sh467}*, *Tg(kdrl:HRAS-mCherry)^{s916}* labelling filamentous actin (F-actin) and EC membrane, we observed that F-actin co-localized with *kugel*n, especially at the *kugel* “neck” (Fig 3B). Time-lapse microscopy revealed this enrichment of F-actin at the *kugel* neck to be highly dynamic (Movie EV3).

To further examine the contents of *kugel*n, we imaged the double-transgenic *Tg(fli1a:eGFP)^{y1}*, *Tg(kdrl:HRAS-mCherry)^{s916}* that labels the EC cytosol and membrane. We were unable to visualize cytosolic GFP within *kugel*n, indicating they contain little if any cytoplasm (Fig 3C).

To further characterize the content inside and tissue surrounding *kugel*n, we examined the triple-transgenic *Tg(gata1:dsRed)*, *Tg(nbt:GCaMP3)*, *Tg(kdrl:HRAS-mCherry)^{s916}* that labels red blood cells (RBCs), developing neurons and EC membrane. RBCs were never observed within *kugel*n. Examination of neurons showed an exclusion of neural tissue (Fig 3D), confirming *kugel*n displace rather than include neural tissue.

***Kugel* formation is reduced by F-actin or Myosin II inhibition**

Since F-actin was enriched at *kugel* necks, we examined whether this was necessary for growth and/or maintenance of *kugel*n. Thus, actin polymerization was inhibited by application of Latrunculin B. This led to a significant increase of number of *kugel*n per embryo (Fig 3E; $P = 0.0041$), but a significant decrease in *kugel* diameter (Fig 3F; $P = 0.0164$).

The role of Myosin II was investigated by chemical inhibition by Blebbistatin treatment. This significantly reduced the number of *kugel*n per embryo (Fig 3G; $P < 0.0001$) but did not affect *kugel*n diameter (Fig 3H; $P = 0.3731$).

The finding that F-actin inhibition increased, while Myosin II inhibition decreased, *kugel* number is consistent with the effect of these manipulations on cellular blebs [13], suggesting some shared mechanisms of *kugel* and bleb biogenesis.

Blood flow is not required for *kugel* formation, maintenance, retraction or oscillation

To study the impact of blood flow and blood pressure, we performed exsanguination by cardiac puncture to reduce blood pressure and flow to zero. Imaging the same animals pre- and post-exsanguination showed no effect on *kugel* size or shape (Fig 4A and B), suggesting neither flow nor pressure are needed to maintain *kugel*n once they have formed. To confirm this, cardiac contraction was temporarily stopped by high-dose Tricaine application and time-lapses acquired. Despite absent blood flow, *kugel*n still developed, changed shape and retracted (Fig 4C and D) as seen under normal blood flow conditions.

We next performed microangiography with fluorescent dextran to investigate whether *kugel*n were perfused by blood or communicated with the lumen of the parent vessel. No entry of dextran into *kugel*n was observed (Fig 4E), suggesting no such communication existed, at least after *kugel*n were formed.

Lastly, we prevented the development of heart contraction by morpholino (MO) knockdown of cardiac troponin 2a (*tnnt2a*) [25–27]. This induced a significant decrease in number of *kugel*n per embryo (Fig 4F; $P < 0.0001$).

Together, these data suggest that blood flow is not the driving mechanism of *kugel* formation, retraction or oscillation, but that vessels that have never experienced flow do not form *kugel*n.

Altered membrane permeability or osmotic pressure does not affect *kugel* formation or diameter

Since DMSO increases membrane permeability [28], we examined whether this had an impact on *kugel* formation. We incubated embryos for 24 h in 2.5% DMSO and found no significant difference in *kugel* number (Fig EV2A; $P = 0.1596$) or diameter (Fig EV2B; $P = 0.3665$).

As osmotic pressure increases cellular bleb formation and platelet ballooning [13,16], we examined whether *kugel*n were affected by increased osmotic pressure. Embryos were incubated for 24 h in a 40 mM glucose solution. No significant difference was found in *kugel* number (Fig EV2C; $P = 0.7371$) or diameter (Fig EV2D; $P = 0.7060$).

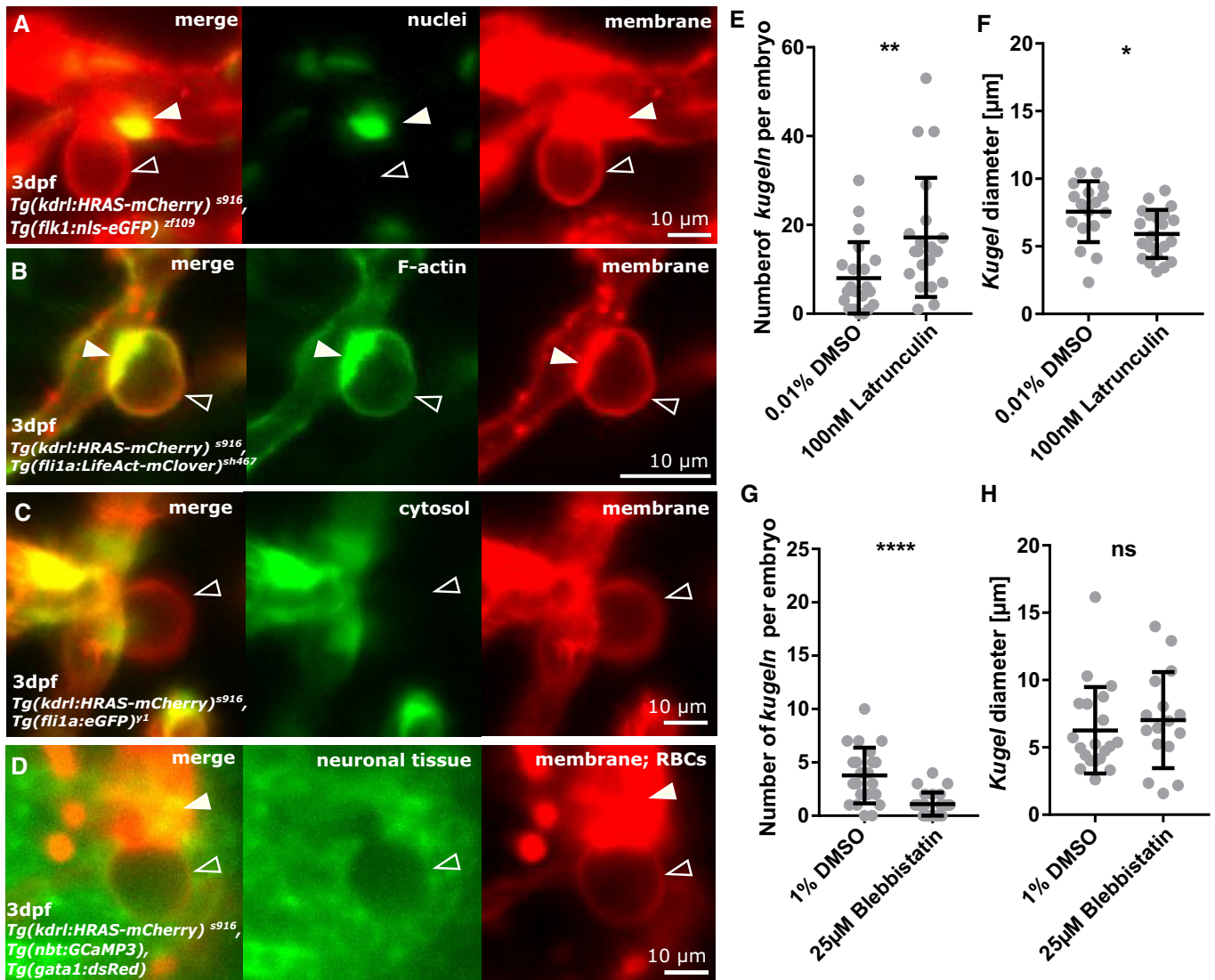


Figure 3. Endothelial *kugeln* are non-nucleated with a filamentous actin-enriched neck.

- A** Double transgenic visualizing endothelial membrane (red) and endothelial nuclei (green). Endothelial nuclei (arrowhead) were observed close to but never within the *kugel* (unfilled arrowhead).
- B** Double transgenic showing endothelial membrane (red) and endothelial F-actin (green). F-actin was found to localize at the neck of the *kugeln* (arrowhead; see also: Movie EV3).
- C** Double transgenic showing endothelial membrane (red) and endothelial cytoplasm (green). The cytoplasmic reporter was visible in the parent vessel but not in the *kugel* (unfilled arrowhead).
- D** Triple transgenic showing endothelial membrane (red), neurons (green) and erythrocytes (red). Surrounding neurons were excluded from the volume of the *kugel* (unfilled arrowhead), and erythrocytes were not observed inside *kugeln* (arrowhead).
- E** Treatment with the inhibitor of actin polymerization Latrunculin B statistically significantly increased number of *kugeln* per embryo (100 nM 1 h; ** $P = 0.0041$; control $n = 21$ embryos 8.05 ± 1.76 (mean \pm s.e.m.); Latrunculin $n = 21$ embryos 17.19 ± 2.93 (mean \pm s.e.m.); 4 dpf; three experimental repeats; Mann–Whitney U -test).
- F** Latrunculin B treatment statistically significantly reduced *kugel* diameter (* $P = 0.0164$; control $n = 169$ *kugeln* from 21 embryos 7.56 ± 2.25 (mean \pm s.e.m.); Latrunculin $n = 361$ *kugeln* from 21 embryos 5.91 ± 1.78 (mean \pm s.e.m.); 4 dpf; three experimental repeats; Student's t -test).
- G** Treatment with the Myosin II inhibitor Blebbistatin statistically significantly reduced number of *kugeln* per embryo (25 µM 1 h; **** $P < 0.0001$; control $n = 22$ embryos 3.77 ± 0.56 (mean \pm s.e.m.), Blebbistatin $n = 24$ embryos 1.08 ± 0.22 (mean \pm s.e.m.); 3 dpf; three experimental repeats; Mann–Whitney U -test).
- H** Blebbistatin treatment had no effect on *kugel* diameter ($P = 0.3731$; control $n = 83$ *kugeln* from 22 embryos 6.27 ± 0.72 (mean \pm s.e.m.), Blebbistatin $n = 26$ *kugeln* from 24 embryos 7.02 ± 0.89 (mean \pm s.e.m.); 3 dpf; three experimental repeats; Mann–Whitney U -test).

Lymphatic cells did not interact with *kugeln*

Next, we investigated the relationship between *kugeln* and the meningeal population of lymphatic cells, brain lymphatic

endothelial cells (BLECs) [14]. We first investigated whether BLECs interacted physically with *kugeln* in the double-transgenic *Tg(kdr1:HRAS-mCherry)^{s916}*, *Tg(fli1a:Lifeact-mClover)^{sh467}*, which allowed us to visualize BLECs as mClover-positive but mCherry-negative

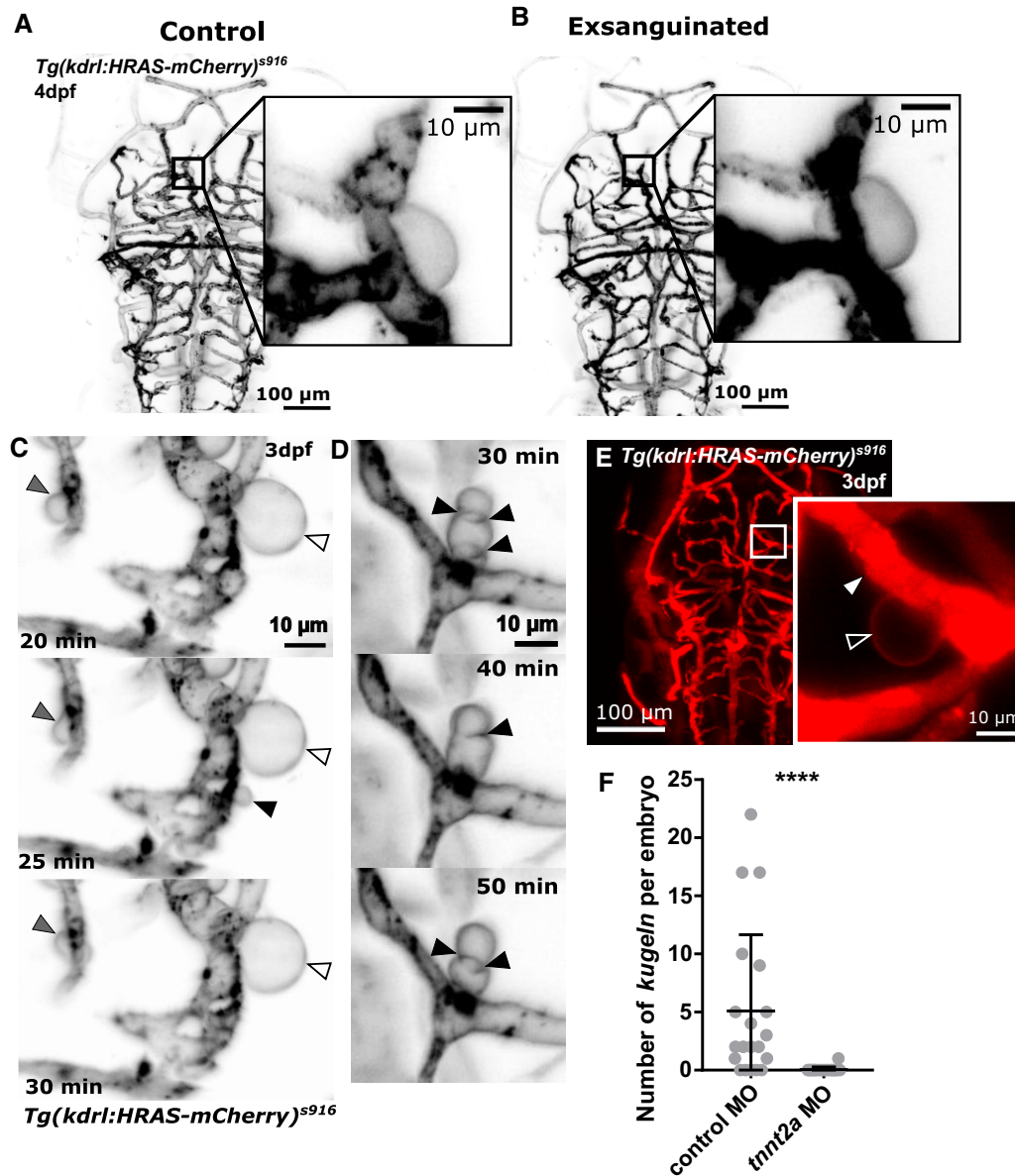


Figure 4. The relationship between endothelial kugeln and blood flow.

A MIP of the cerebral vessels of a 4 dpf embryo before exsanguination (grey LUT; inverted).
 B MIP of the same embryo after exsanguination, which did not alter *kugel* size.
 C Time-lapse imaging of an embryo with transiently halted cardiac contraction (using Tricaine). Despite absent blood flow *kugel* still changed shape (grey arrowhead), retained shape (white arrowhead) or protruded and retracted (black arrowhead; time post cessation of flow is indicated on micrographs; 3 dpf; grey inverted LUT).
 D Time-lapse of an embryo with transiently halted cardiac contraction as in (C) showed that *kugel* diameter still oscillates (time post cessation of flow).
 E Dextran microangiography filled perfused vessels with dextran (arrowhead), while dextran was not observed to enter *kugel* (unfilled arrowhead).
 F Inhibition of cardiac contraction by *tnnt2a* morpholino (MO) knockdown statistically significantly reduced *kugel* number per embryo (**** $P < 0.0001$; control $n = 20$ embryos 5.10 ± 1.47 (mean \pm s.e.m.), *tnnt2a* MO = 18 embryos 0.06 ± 0.06 (mean \pm s.e.m.); 3 dpf; three experimental repeats; Mann–Whitney *U*-test).

structures (Fig 5A–C). BLECs were observed to be at a different anatomical depth than *kugeln* (Fig 5D), and no direct interaction between BLECs and *kugeln* was ever observed ($n = 21$, 4 dpf embryos; three experimental repeats).

To examine whether lymphatics are required for *kugeln* formation, BLEC formation was inhibited by MO knockdown of *ccbe1* (Fig 5E) [21]. This had no effect on either number of *kugeln* per embryo (Fig 5F) or *kugel* diameter (Fig 5G).

These findings were confirmed by imaging the double-transgenic *Tg(kdrl:HRAS-mCherry)^{s916}, Tg(flt4^{BAC}:mCitrine)^{hu7135}*, which more specifically labels BLECs (Fig EV3A). Again, *ccbe1* MO knockdown had no effect on *kugel* number (Fig EV3B and C; $P = 0.1472$) or diameter (Fig EV3D; $P = 0.0962$).

Next, we examined whether *kugeln* serve an uptake function, similar to BLECs [14]. We studied whether IgG-conjugated Alexa Fluor 674, injected into the tectum, would be taken up by *kugeln*.

While BLECs readily took up the IgG-conjugated Alexa, this was not observed in *kugel*n (Fig 5H; 140 *kugel*n from 17 4 dpf embryos; Fig EV3E 52 *kugel*n from five 5 dpf embryos).

Macrophages do not interact with *kugel*n

Since macrophages interact with vessels undergoing anastomosis [29], we imaged the triple-transgenic line *Tg(fms:GALA.VP16)¹¹⁸⁶, Tg(UAS-E1b:nfsB.mCherry)¹¹⁴⁹, Tg(kdrl:HRAS-mCherry)⁵⁹¹⁶*, which labels both macrophages and endothelial cells with mCherry (Fig 6A). To distinguish the anatomical depth of *kugel*n and macrophages, depth coding was performed; also, macrophages could be identified by cell shape and movement between frames of time-lapses (Fig 6B). We never observed direct interaction of macrophages with *kugel*n (Fig 6C; Movie EV4; $n = 21$ *kugel*n in eight 3 dpf embryo), suggesting that *kugel*n do not directly respond to local inflammation and/or recruitment of macrophages [29].

Number of *kugel*n is increased by VEGF inhibition, and while *kugel*n contain NO, they do not require NO synthase for their formation

Due to the essential role of VEGF in angiogenesis, we examined the effect of VEGF signalling inhibition on *kugel* formation [17,30]. The VEGF inhibitor AV951 significantly increased the number of *kugel*n per embryo (Fig 7A; $P < 0.0001$), without affecting *kugel* diameter (Fig 7B; $P = 0.7890$). Since nitric oxide (NO) is induced by VEGF [31], we incubated embryos with the vital dye DAF-FM, which fluoresces green in contact with NO [23,33]. We found 57.76% of *kugel*n (118 of 205 *kugel*n; 22 embryos) were fluorescent, indicating high levels of NO reactivity (Fig 7C). To identify at which point *kugel*n begin to contain NO, we performed time-lapse microscopy of *kugel* formation after DAF-FM staining and found NO reactivity was detectable at the start of *kugel* formation (Fig 7D). Because DAF-FM can fluoresce in acidic environments even in the absence of NO [34], we performed LysoTracker staining, which visualizes acidic cell compartments [35,36]. Only 17.08% of *kugel*n were positive for LysoTracker (Fig 7E; 62 of 363 *kugel*n; 22 embryos), suggesting that *kugel*n do indeed contain NO.

We examined whether nitric oxide synthase (NOS) was required for *kugel* formation by application of the NOS inhibitor L-NAME [31,37]. Neither *kugel* number (Fig 7F; $P = 0.4870$) nor diameter were significantly altered by L-NAME treatment (Fig 7G; $P = 0.4161$).

Notch signalling is required for *kugel* formation

Having found that VEGF signalling negatively regulates *kugel* formation, we studied its counter-part Notch [19,38,39]. Pharmacological inhibition of Notch signalling by DAPT significantly reduced *kugel* number (Fig 8A; $P < 0.0001$), while not significantly affecting *kugel* diameter (Fig 8B; $P = 0.0832$).

Because these data suggested Notch signalling was required for *kugel* formation, we examined expression of the Notch ligand *dll4* in the double-transgenic reporter line *Tg(dll4in3:eGFP), Tg(kdrl:HRAS-mCherry)⁵⁹¹⁶*. Upon visual examination, no differential *dll4* levels were observed in proximity to *kugel*n or *kugel*-parent-vessels (Fig 8C), suggesting that *dll4* was not locally up- or down-regulated nearby *kugel*n.

To further examine Notch signalling, we utilized the transgenic *Tg(TP1bglob:VenusPest)⁵⁹⁴⁰, Tg(kdrl:HRAS-mCherry)⁵⁹¹⁶*. Expression of VenusPest is under the control of the synthetic Notch-responsive element *TP1* and was found to mainly be expressed in the midbrain and to a lesser extent in the hindbrain; but, again, no differential expression was seen adjacent to *kugel*n, in *kugel*n or in *kugel*-parent-vessels (Fig 8D).

To determine which component of the Notch pathway is required for *kugel*n formation, we examined the effect of morpholino knockdown of the Notch ligands *dll4*, *notch1b*, *jagged-1a* and *jagged-1b*. Knockdown of *dll4* or *jagged-1b* did not significantly affect *kugel* number or diameter (Fig EV4A, B, G, and H). However, morpholino knockdown of *notch1b* significantly reduced *kugel*n number (Fig EV4C; $P = 0.0008$), without affecting diameter (Fig EV4D). Conversely, *jagged-1a* knockdown significantly increased *kugel* diameter (Fig EV4F; $P = 0.0097$) without affecting *kugel*n number (Fig EV4E).

Both inhibition and activation of Wnt signalling increase *kugel* number

Since the dorsal central cranial vessels are dependent on Wnt signalling [20,40,41], the impact of Wnt signalling on *kugel*n formation was studied. Inhibition of Wnt signalling was achieved by application of XAV-939 [42]. This significantly increased number of *kugel*n per embryo (Fig 8E; $P = 0.0003$), while not affecting *kugel* diameter (Fig 8F; $P = 0.4098$).

Interestingly, activation of Wnt signalling by application of the GSK3 inhibitor XV, which prevents β -catenin phosphorylation [43], also significantly increased number of *kugel*n per embryo (Fig 8G; $P < 0.0001$), while again not affecting *kugel* diameter (Fig 8H).

Figure 5. *Kugel*n do not interact with brain lymphatic endothelial cells (BLECs) in *Tg(fli1a:LifeAct-mClover)^{sh467}, Tg(kdrl:HRAS-mCherry)⁵⁹¹⁶*, nor do they take up injected IgG-conjugated Alexa 674.

- Kugel*n were studied in the double-transgenic *Tg(fli1a:LifeAct-mClover)^{sh467}, Tg(kdrl:HRAS-mCherry)⁵⁹¹⁶*.
- BLECs were mClover-positive and mCherry-negative (BLECs—black arrowheads; *kugel*n—white arrowheads).
- No direct physical interaction between *kugel*n (BLECs—black arrowheads; *kugel*n—white arrowheads) and BLECs was observed ($n = 21$ 4 dpf embryos; three experimental repeats).
- Depth-coded MIPs showed that BLECs and *kugel*n are present on different anatomical planes (depths; purple ventral (v), white dorsal (d); BLECs—black arrowheads; *kugel*n—white arrowheads).
- Ccbe1* morpholino (MO) injection led to a loss of lymphatics (white arrowhead).
- Kugel* number was not statistically significantly altered by *ccbe1* morpholino (MO) knockdown ($P = 0.3496$; control MO $n = 22$ embryos 0.95 ± 0.28 (mean \pm s.e.m.), *ccbe1* MO $n = 23$ embryos 0.57 ± 0.14 (mean \pm s.e.m.); 3 dpf; three experimental repeats; Mann–Whitney *U*-test).
- Kugel* diameter was not statistically significantly altered by *ccbe1* MO knockdown ($P = 0.8783$; control MO $n = 21$ *kugel*n from 22 embryos 7.75 ± 1.29 (mean \pm s.e.m.), *ccbe1* MO $n = 13$ *kugel*n from 23 embryos 8.93 ± 2.35 (mean \pm s.e.m.); 3 dpf; three experimental repeats; Mann–Whitney *U*-test).
- Injection of IgG-conjugated Alexa 647 into the tectum showed no uptake (blue; unfilled arrowhead) by *kugel*n (white arrowhead; 140 *kugel*n from 17 4 dpf embryos; two experimental repeats).

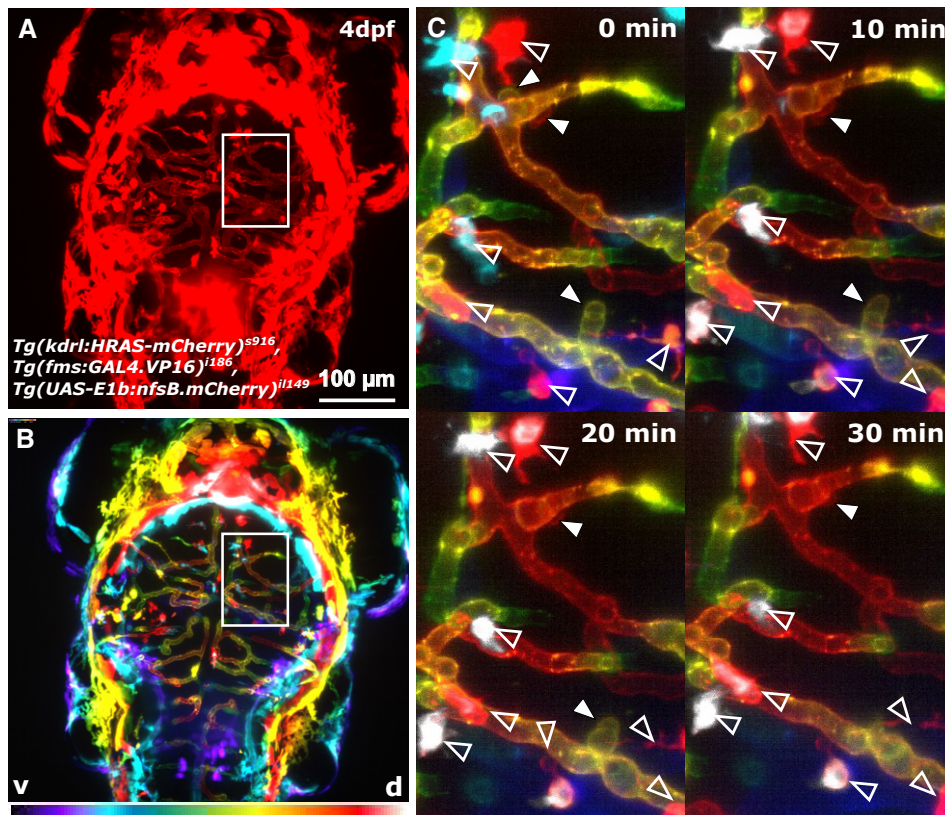


Figure 6. Kugeln do not interact with macrophages.

- A The possible interaction of macrophages with *kugeln* was studied in the transgenic *Tg(kdr1:HRAS-mCherry)^{S916}*, *Tg(fms:GAL4.VP16)^{I186}*, *Tg(UAS-E1b:nfsB.mCherry)^{I149}*, visualizing macrophages and the vasculature simultaneously.
- B Coloured depth coding indicates the different anatomical depths of *kugeln* and macrophages (ventral purple, dorsal white).
- C Maximum intensity projections of z-stacks acquired every 10 min during a time-lapse showed no interaction of macrophages (unfilled arrowhead) with *kugeln* (filled arrowhead; $n = 21$ *kugeln* in eight 3 dpf embryos). Macrophages are all white, indicating they are on a different z-plane to the vessels seen.

Discussion

We here describe a previously unreported form of EC behaviour in zebrafish found only on the cerebral vessels. We believe that *kugeln* were not described previously due to their highly dynamic nature and low number per animal. Our discovery was greatly facilitated by state-of-the-art light sheet microscopy that provided the required imaging speed and 3D imaging capability. Moreover, *kugeln* are only detectible in EC membrane-tagged reporter lines, whereas many previous studies have utilized cytoplasmic reporter lines that we have shown do not label *kugeln*. However, retrospective analysis of multiple datasets generated in Sheffield, Münster and Dresden confirmed their existence in unrelated zebrafish colonies, and they were detected using three different approaches to label endothelial membrane. This coupled with their restriction to the cerebral vessels, and their regulation by known biological pathways such as actin polymerization as well as VEGF, Notch and Wnt signalling confirms that *kugeln* formation is a real phenomenon.

Kugeln are reliably observed from 3 dpf onwards but are not present at 32 hpf (2.3 dpf). The reason for this timing of onset is not presently known and may relate to a waning of VEGF signalling (which would otherwise suppress *kugeln* formation),

increasing Notch signalling in the brain or a required state of maturity of the cerebral vessels. However, *kugeln* persist as late as 28 dpf, so they do not represent a purely embryonic phenomenon. Unfortunately, the increasing size and opacity of zebrafish after 28 dpf have prevented us from imaging older animals or adults.

As well as representing the first description of *kugeln*, our manuscript has taken important steps towards understanding their biogenesis. Although *kugel* diameter greatly exceeds that of previously described vesicular membrane structures, *kugel* biogenesis shares common features with cellular blebs such as a requirement for actin polymerization and Myosin II [13]. Despite an appearance reminiscent of vascular aneurysms, unlike these *kugeln* are not multicellular and their formation appears not to be driven by blood flow. Because complete absence of blood flow throughout development prevents *kugeln* formation, we speculate that some exposure to blood flow may be needed to establish EC properties in the cerebral vessels such as polarity, shear stress responses and lumenization [4,44], to allow *kugeln* to form.

Although VEGF, Notch and Wnt signalling have all been previously shown to play central roles in angiogenesis [17,19,20,27,38,45], they have not previously been implicated in

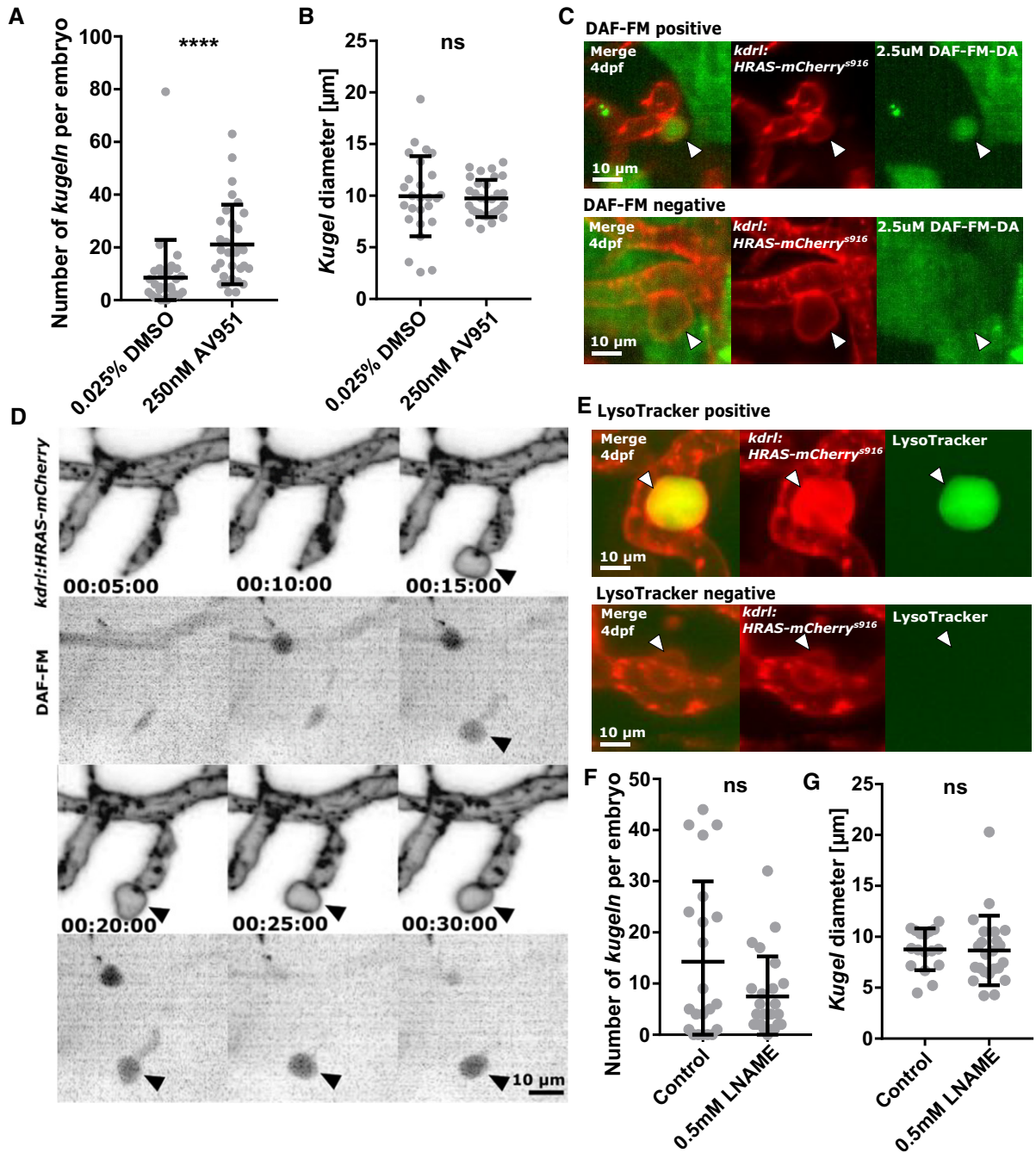


Figure 7. Kugel number is increased by VEGF inhibition, and kugeln contain NO.

A VEGF inhibition by 2 h treatment with AV951 statistically significantly increased *kugel* number (**** $P < 0.0001$; DMSO control $n = 30$ embryos 8.53 ± 2.62 (mean \pm s.e.m.); AV951 $n = 31$ embryos 21.10 ± 2.71 (mean \pm s.e.m.); 4 dpf; four experimental repeats; Mann–Whitney U -test).

B Mean *kugel* diameter was not statistically significantly different after AV951 treatment ($P = 0.7890$; DMSO control $n = 243$ *kugeln* from 30 embryos 9.94 ± 0.76 (mean \pm s.e.m.); AV951 $n = 652$ *kugeln* from 31 embryos 9.73 ± 0.32 (mean \pm s.e.m.); 4 dpf; four experimental repeats; Student's t -test).

C DAF-FM staining, a vital dye for nitric oxide (NO), showed that 57.56% of *kugeln* were positive for nitric oxide reactivity (2.5 μ M incubation from 96 to 102 hpf; $n = 22$ 4 dpf embryos; 118 of 205 *kugeln* filled; three experimental repeats). Images show representative “filled” (DAF-FM positive) and “unfilled” (DAF-FM negative) *kugeln*.

D Time-lapse acquisition with DAF-FM revealed that *kugeln* contained NO early in their biogenesis (grey LUT; inverted).

E Application of LysoTracker, a vital dye that stains lysosomes or acidic compartments, showed that 17.08% of *kugeln* contained acidic contents (8.33 μ M; 96–101 hpf; $n = 22$ 4 dpf embryos; 62 of 363 *kugeln* filled; 3 experimental repeats). Images show representative “filled” (LysoTracker positive) and “unfilled” (LysoTracker negative) *kugeln*.

F The nitric oxide synthase (NOS) inhibitor L-NAME had no statistically significant effect on *kugel* number per embryo (0.5 mM L-NAME 18 h; $P = 0.4870$; control $n = 22$ embryos 14.27 ± 3.35 (mean \pm s.e.m.), L-NAME $n = 24$ embryos 7.46 ± 1.61 (mean \pm s.e.m.); 4 dpf; three experimental repeats; Mann–Whitney U -test).

G Diameter of *kugeln* was not affected by L-NAME ($P = 0.4161$; control $n = 315$ *kugeln* from 22 embryos 8.77 ± 0.49 (mean \pm s.e.m.), L-NAME $n = 179$ *kugeln* from 24 8.66 ± 0.71 (mean \pm s.e.m.); 4 dpf; three experimental repeats; Mann–Whitney U -test).

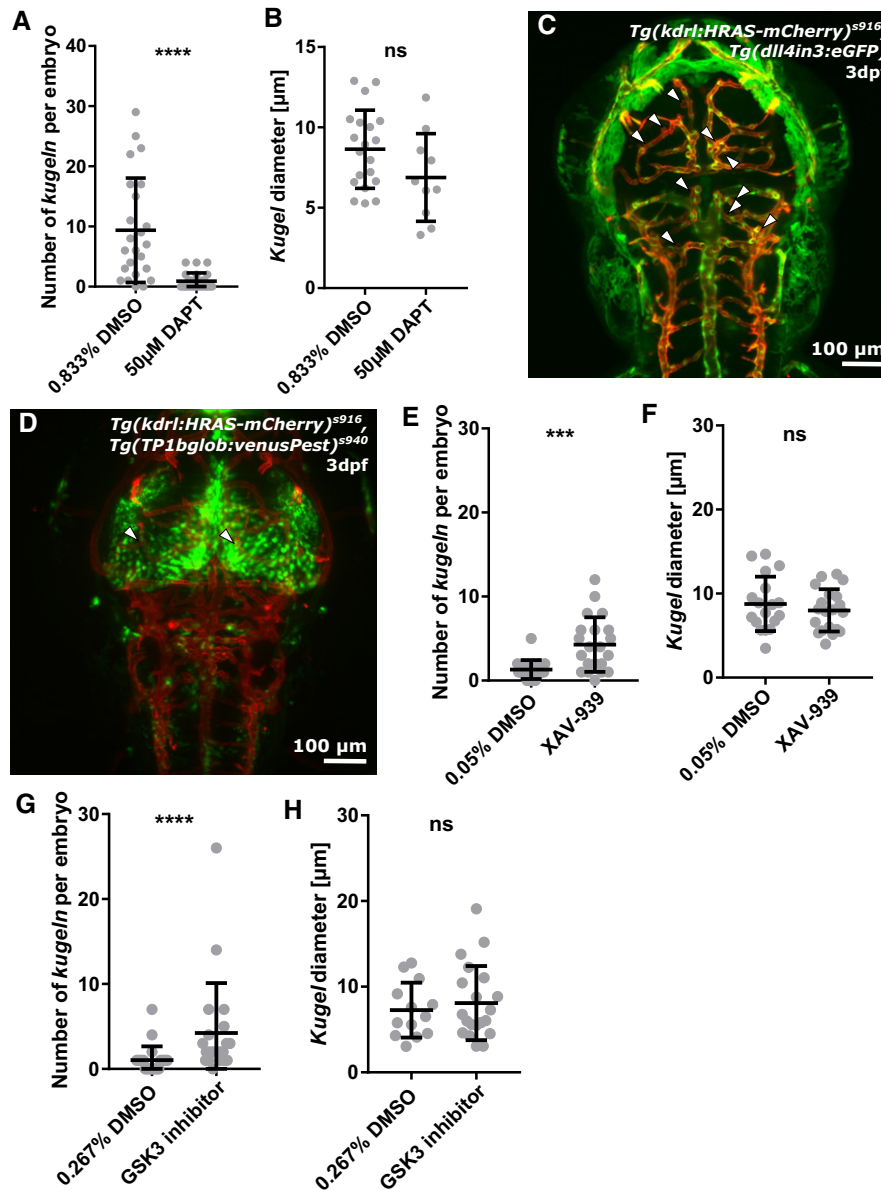


Figure 8. *Kugel* number is decreased by Notch inhibition but increased by Wnt inhibition or activation.

- A *Kugel* number was significantly decreased by inhibition of Notch signalling by 12 h treatment with 50 μM DAPT (**** $P < 0.0001$; control $n = 24$ embryos 9.38 ± 1.77 (mean \pm s.e.m.), DAPT $n = 24$ embryos 0.92 ± 0.28 (mean \pm s.e.m.); 4 dpf; three experimental repeats; Mann–Whitney U -test).
- B Mean *kugel* diameter was not statistically significantly altered by DAPT treatment ($P = 0.0832$; control $n = 225$ *kugelIn* from 24 embryos 8.64 ± 0.54 (mean \pm s.e.m.); DAPT $n = 22$ *kugelIn* from 24 embryos 6.88 ± 0.86 (mean \pm s.e.m.); 4 dpf; three experimental repeats; Student's t -test).
- C A transgenic *dll4* reporter line showed no indication of different *dll4* expression at the sites of *kugelIn* (white arrowheads pointing to *kugelIn*; $n = 122$ *kugelIn* from 23 3 dpf embryos; two experimental repeats).
- D Studying Notch signalling in the Notch reporter line *Tg(TP1bglob:venusPest)^{s940}*, showed high Notch levels in the midbrain, but, again, no difference in expression at the sites of *kugelIn* ($n = 45$ *kugelIn* from 19 4 dpf embryos; two experimental repeats).
- E *Kugel* number was statistically significantly increased by inhibition of Wnt signalling by 4 h treatment with 10 μM XAV-939 (*** $P = 0.0003$; control $n = 22$ embryos 1.32 ± 0.24 (mean \pm s.e.m.); XAV-939 $n = 21$ embryos 4.29 ± 0.71 (mean \pm s.e.m.); 3 dpf; three experimental repeats; Mann–Whitney U -test).
- F *Kugel* diameter was not statistically significantly altered by XAV-939 ($P = 0.4098$; control $n = 29$ *kugelIn* from 22 embryos 8.78 ± 0.76 (mean \pm s.e.m.); XAV-939 $n = 90$ *kugelIn* from 21 embryos 7.99 ± 0.56 (mean \pm s.e.m.); 3 dpf; three experimental repeats; Student's t -test).
- G *Kugel* number was statistically significantly increased by activation of Wnt signalling by 10 μM GSK3 inhibitor XV ($p = 0.0359$; control $n = 22$ embryos 1.04 ± 0.34 (mean \pm s.e.m.); GSK3 inhibitor $n = 21$ embryos 4.24 ± 1.28 (mean \pm s.e.m.); 3 dpf; three experimental repeats; Mann–Whitney U -test).
- H The diameter of *kugel* was not statistically significantly altered by GSK3 inhibition ($p = 0.5555$; control $n = 23$ *kugelIn* from 22 embryos 7.26 ± 0.89 (mean \pm s.e.m.); GSK3 inhibitor $n = 89$ *kugelIn* from 21 embryos 8.09 ± 0.97 (mean \pm s.e.m.); 3 dpf; three experimental repeats; Student's t -test).

vesicle biogenesis. We find that all three of these signalling pathways influence *kugel* formation. VEGF signalling inhibits, while Notch signalling is required for *kugel* formation. Our preliminary morpholino antisense studies suggested *notch1b* but not *dll4* is required for *kugel* formation, and interestingly that perhaps *jagged-1a* may negatively regulate this. However, morpholinos are associated with a significant risk of off-target effects [46] and future studies using other approaches to induce loss of function of these genes will be revealing. For example, an examination of *kugel* formation in stable mutants of these genes would be interesting although it may be challenging to discriminate between the effects of their loss of function on general cerebrovascular development. The recent establishment of endothelial-specific CRISPR interference may also be informative [47].

Our finding that the majority of *kugeln* contained high levels of NO was unexpected as NO is generally considered to passively diffuse from NO-producing cells and no NO-containing organelle has previously been described [48]. We speculate that accumulation of NO in *kugeln* may serve to establish a signalling or storage hub as described for secreted molecules such as *Fgf3* [49]. This would provide a facility to deliver large amounts of NO rapidly. It is interesting that *kugeln* contain NO early in their lifetime, which, when coupled with their lack of cytoplasm, suggests that perhaps their formation might be related to “inflation” with NO, although this might be expected to be inhibited by L-NAME which we did not observe. Furthermore, most, but not all *kugeln* contain NO. It is possible therefore that regression of *kugeln* is associated with emptying of NO from the *kugel*, perhaps by diffusion into the tissue or lumen.

The link between VEGF, NO and *kugeln* is unclear; VEGF induces NO release from ECs [31] but inhibits *kugeln* formation. It has been questioned whether zebrafish possess an orthologue of endothelial nitric oxide synthase (eNOS), but the balance of evidence suggests not [50]. However, zebrafish do possess orthologues for inducible and neuronal NOS and it may be these isoforms that generated the NO we detected [51].

Several key questions remain unanswered by our study. Why are *kugeln* restricted to the cerebral vessels and what is their function? We can presently only speculate, but the dependence of *kugeln* on Notch signalling may provide a clue. The brain is a site of marked Notch pathway activity to which the cerebral vessels are exposed, and this may explain the localization of *kugeln* to these vessels. Several human genetic diseases affecting the cerebral vasculature are linked to the Notch pathway. For example, cerebral autosomal dominant arteriopathy with subcortical infarcts and leukoencephalopathy (CADASIL) is the most common monogenic form of ischaemic stroke and is caused by mutations in the Notch receptor NOTCH [52–54]. Cerebral cavernous malformations (CCMs) are common large vascular cavernomas due to enlarged brain sinusoids. CCMs are caused by mutations in the CCM genes, which form a complex involved in stabilization of endothelial junctions and VEGF signalling [55,56]. Silencing CCM genes reduces Notch signalling, again implicating Notch dysregulation with human genetic cerebrovascular diseases. Since Notch inhibition impairs *kugel* formation, in addition to the fact that *kugeln* occurs in physiologically wild-type (though transgenic) animals, it seems most likely that *kugel* formation plays a positive, though as yet unknown, function in maintaining cerebral vessels. To test this will require discovery of a method to

specifically prevent *kugel* formation in order to test the effect on cerebrovascular function.

It remains to be seen whether *kugeln* exist in mammals. Given the conservation of endothelial behaviour between zebrafish and mammals, we consider this highly likely. Although they have not previously been described, our findings show it is clear that *kugeln* are easy to overlook, particularly on histological examination of mammalian brains, which would easily mistake *kugeln* for capillaries. However, now that their existence is known, the use of membrane-tagged reporters or immunostaining coupled with a marker of perfusion would be expected to reveal whether *kugeln* exist in the mammalian brain.

We conclude that we have uncovered a striking subcellular phenomenon that appears restricted to cerebral vessels, emphasizing that our understanding of the intricate processes during vascular development is far from complete.

Material and Methods

Zebrafish strains, handling and husbandry

Experiments performed at the University of Sheffield conformed to UK Home Office regulations and were performed under Home Office Project Licence 70/8588 held by TJAC. Experiments performed at the Max Planck Institute of Molecular Cell Biology and Genetics in Dresden and the WWU Münster Institute for Cardiovascular Organogenesis and Regeneration conformed to guidelines of the relevant German animal ethics committees.

Maintenance of adult zebrafish in all three fish facilities was conducted according to previously described husbandry standard protocols at 28°C with a 14:10 hours (h) light:dark cycle [57]. Embryos, obtained from controlled pair- or group-mating, were incubated in E3 buffer (5 mM NaCl, 0.17 mM KCl, 0.33 mM CaCl₂, 0.33 mM MgSO₄) with or without methylene blue.

The following zebrafish lines were used; *Tg(kdr:HRAS-mCherry)^{s916}* labels EC membrane [58] (AB background [59]; *Casper* background [60]), *Tg(gata1:dsRed)* labels red blood cells (RBCs) [61], *Tg(fli1aep:CAAX-eGFP)* labels EC membrane [22] (kindly provided by Holger Gerhardt), *Tg(fli1a:eGFP)^{v1}* labels EC cytoplasm [8], *Tg(kdr:nls-eGFP)^{z109}* labels EC nuclei [62], *Tg(fli1a:Lifeact-mClover)^{sh467}* labels endothelial filamentous actin [47], and *Tg(nbt:GCAMP3)* labels neurons [63], *Tg(dll4in3:GFP)* is expressed at sites of expression of the Notch delta-like ligand 4 [45] (kindly provided by the De Val laboratory), *Tg(TP1bglob:VenusPest)^{s940}* labels arterial ECs [64]. BLECs were studied in the double-transgenic lines *Tg(kdr:HRAS-mCherry)^{s916}*, *Tg(flt4^{BAC}:mCitrine)^{hu7135}* [65] and *Tg(kdr:HRAS-mCherry)^{s916}*, *Tg(fli1a:Lifeact-mClover)^{sh467}*. Macrophages were studied in *Tg(fms:GAL4.VP16)ⁱ¹⁸⁶*, *Tg(UAS-E1b:nfsB-mCherry)^{il149}* and *Tg(kdr:HRAS-mCherry)^{s916}* [66]. Transient expression of *Tg(fli1:myr-mCherry)*, labelling EC membrane [30,31], was achieved by injection of plasmid (50 pg) with Tol2 RNA (75 pg).

Image acquisition

Datasets in Sheffield were obtained using a Zeiss Z.1 light sheet microscope with a water-dipping detection objective (Plan-

Apochromat 20×/1.0 Corr nd = 1.38) and a scientific complementary metal-oxide semiconductor (sCMOS) detection unit. Data were acquired with activated pivot scan, dual-sided illumination and online fusion; properties of acquired data are as follows: 0.7× zoom, 16bit image depth, 1,920 × 1,920px image size and minimum z-stack interval (approx. 0.33 × 0.33 × 0.5 μm). Green and red fluorophores were excited using 488 nm and 561 nm laser, respectively. Used filters in sequential tracks for multi-colour images were LP560 for both and BP505-545 and LP585, respectively. Samples were embedded in 1% or 2% LMP-agarose containing 200 mg/l Tricaine (MS-222, Sigma). The image acquisition chamber was filled with E3 plus Tricaine (200 mg/ml) and maintained at 28°C.

Light sheet datasets in Dresden were obtained with a custom-built multidirectional SPIM (mSPIM) set-up [67]. The dorsum of the embryo head was imaged every 2.5 min over 2 days with dual illumination and 3 μm z-spacing. The mSPIM set-up was equipped with a Coherent Sapphire 561 nm laser, two Zeiss 10×/0.2 illumination objectives, an UMPlanFL N Olympus 20×/0.5 NA detection objective and an Andor iXon 885 EM-CCD camera. To cover the cerebrovascular region, several regions were imaged and later stitched using custom image processing plug-ins in Fiji [68] based on the stitching tool from Stefan Preibisch [69]. Samples were mounted in fluorinated propylene ethylene (FEP) tubes according to established mounting protocols [70]. The FEP tubes were coated with 3% methyl cellulose and filled with 0.1% low-melting agarose containing 200 mg/l Tricaine to immobilize the zebrafish embryos during time-lapse imaging.

Data acquisition for the study of BLECs was performed at the University of Münster using a Leica SP8 microscope with a 40× water immersion objective (0.75× zoom) exciting with a 514 nm argon laser, 561 nm diode-pumped solid-state laser, 633 nm helium-neon and 514/561/633 beam splitters. Properties of data acquired were as follows: 16bit image depth, 1,024 × 1,024 px image size and 1 μm minimum z-stack interval. Sample embedding was performed in 0.8% low-melting agarose with 200 mg/l Tricaine.

Microangiography

Vascular perfusion was visualized as previously described [71,72], using 20 μg dextran tetramethylrhodamine (2,000,000 molecular weight, Thermo Fisher) at a concentration of 10 mg/μl (2 nl injection volume).

Exsanguination and cessation of cardiac contraction

Exsanguination was achieved by mechanical opening of the heart with forceps. Temporary cessation of cardiac contraction was induced by treatment with 3.7 mM Tricaine in E3. After 20 min incubation and 30–40 min image acquisition, samples were placed in E3 without Tricaine until full recovery of cardiac contraction to confirm non-lethality of Tricaine exposure.

Morpholino antisense oligomer-induced gene knockdown

Inhibition of induction of cardiac contraction was achieved by injection of an ATG blocking morpholino (MO) against cardiac troponin

2 (*tnnt2a*) at 1.58 ng/embryo (Genetools, LLC; sequence 5'-CATGTTTGTCTCT GATCTGACACGCA-3') [25].

Development of BLECs was inhibited by injection of an ATG blocking MO against collagen and calcium-binding EGF-like domain 1 (*ccbe1*) at 5 ng/embryo (Genetools, LLC; sequence 5'-CGGGTA GATCATTTCAGACACTCTG-3') [73].

The role of Notch signalling was investigated by injection of an ATG blocking MO against the following components: delta-like ligand 4 (*dll4*; 3 ng; Genetools, LLC; sequence 5'-GAGAAAGTGAGC CAAGCTGCCATG-3') [74], *jagged-1a* (*jag1a*; 0.1 ng; 5'-GTCTG TCTGTGTGTCTGTCGCTGTG-3'; Genetools, LLC) [74], *jagged-1b* (*jag1b*; 0.8 ng; Genetools, LLC; sequence 5'-CTGAACTCCGTCGCA GAATCATGCC-3') [74] and *notch 1b* (0.25 ng; Genetools, LLC; sequence 5'-GTTCTCCGGTTACCTGGCATAACAG-3') [75].

Control MO injection was performed, according to the same protocol, with final concentrations as above (5'-CCTCTTACCT CAGTTATTATA-3'; Genetools, LLC). All MO injections were conducted at one-cell stage using phenol red as injection tracer.

Tectum injections

Possible *kugel* scavenging activity was examined by injection of IgG-conjugated 150 kDa Alexa Fluor 674 (0.2 mg/ml, Thermo Fisher) into the tectum and ventricle at 3 dpf, as previously described [14].

Chemical treatments

Actin polymerization was inhibited using 100 nM Latrunculin B for 1 h between 96 and 97 hpf (Sigma-Aldrich) [76].

Myosin II was inhibited using 25 μM Blebbistatin (with 1% DMSO in end solution for solubility) for 1 h between 75 and 76 hpf (Sigma) [77].

VEGF signalling was inhibited using VEGF receptor inhibitor AV951 [78] at 250 nM for 2 h from 96 to 98 hpf (Selleckchem; S1207; Tivozanib—AVEO pharmaceuticals).

Notch signalling was inhibited using 50 μM DAPT (Sigma-Aldrich) for 12 h from 84 to 96 hpf [79].

Wnt signalling was inhibited using 10 μM XAV-939 for 4 h from 72 to 76 hpf (Sigma) [42]. Wnt signalling activation was achieved by 10 μM GSK-3 inhibitor XV for 4 h from 72 to 76 hpf (Merck) [43].

Control groups for the above experiments were performed using the same concentration and duration of DMSO in the active treatments.

Inhibition of nitric oxide synthase (NOS) was achieved by 0.5 mM L-NAME (Sigma-Aldrich) dissolved in E3 for 18 h from 3 to 4 dpf [31]. Controls were incubated in E3.

The impact of osmotic pressure on *kugeln* was studied using 40 mM glucose treatment for 24 h from 72 to 96 hpf (Sigma). Controls were incubated in E3.

The impact of cell membrane permeability on *kugeln* was studied by application of 2.5% (v/v) DMSO for 24 h from 72 to 96 hpf (Sigma). Controls were incubated in E3.

Vital dye staining

In vivo visualization of nitric oxide (NO) was performed using 2.5 μM DAF-FM-DA (Molecular Probes; D23844) [32] for 6 h in

4 dpf embryos (96–102 hpf). DMSO control was performed at the same concentration and duration. To visualize acidic cellular compartments, LysoTracker Green (Molecular Probes; L7526 DND-26) was applied for 5 h (96–101 hpf) at a concentration of 8.33 μ M in E3 [35,36]. Controls were incubated in E3.

Image analysis and representation

Images were analysed using open-source software Fiji [68]. Kymographs were produced via stack reslicing to study diameter changes of *kugeln* over time. To visualize data, maximum intensity projections (MIP) were generated and displayed using either grey (single channel) or red/green/blue (multi-channel) colour representations. Z-stack depth coding was conducted via hyper-stack time-coding. Intensity inversion was applied, as appropriate, to give the clearest rendering of relevant structures. Time-lapse data were displayed using MIPs. 3D image reconstruction for 360-degree rotation was performed using Arivis software.

Statistical analysis

All animals with sufficient image quality to be analysed were included. Animals were randomly allocated to treatment groups. Imaging and data analysis was performed unblinded to treatment allocation since the effects of treatment were usually obvious from the appearances of the micrographs.

Normality of data was tested using D'Agostino-Pearson omnibus test. Statistical analysis of normally distributed data was performed using a one-way ANOVA to compare multiple groups or Student's *t*-test to compare two groups. Non-normally distributed data were analysed with a Kruskal–Wallis test to compare multiple groups, or Mann–Whitney *U*-test to compare two groups. Diameter of *kugeln* is shown as average of all *kugeln* per embryo, unless otherwise indicated. Analysis was performed in GraphPad Prism Version 7 (GraphPad Software, La Jolla California USA). *P*-values are indicated as follows: **P* < 0.05, ***P* < 0.01, ****P* < 0.001, *****P* < 0.0001. Data represent mean and standard deviation (s.d.), if not otherwise stated. Image representation was performed using Inkscape (<https://www.inkscape.org>).

Data availability

All data are available on request.

Expanded View for this article is available online.

Acknowledgements

We thank the Bateson Centre aquarium facility for excellent zebrafish husbandry and guidance on experiments. We are grateful for the *Tol2-flil1a:myr-mCherry* plasmid supplied by Naoki Mochizuki. We thank Emily Noël, the Perak laboratory Sheffield and Henry Roehl for sharing chemical compounds. We thank Alex McGown for advice on tectum injections. This work was supported by a University of Sheffield, Department of Infection, Immunity and Cardiovascular Disease, Imaging and Modelling Node Studentship awarded to ECK, and by a DFG grant to SSM (SCHU 1228/2-2). RBM is funded by a Wellcome Trust Seed award (210152/Z/18/Z). The Zeiss Z1 LSFM was funded via British Heart Foundation Infrastructure Award IG/15/1/31328 awarded to TJAC

and RNW. We are grateful to Professor Holger Gerhardt and Professor Alastair Poole for discussions and advice.

Author contribution

Funding Acquisition, RBM, JH, SS-M, RNW, PA and TJAC; Investigation, Validation and Data Curation, ECK, ML, SD, KC, AMS, VS, KP; Formal Visualization and Analysis, ECK; Resources, RBM, JH, SS-M, RNW, PA and TJAC; Project Administration, ECK, KP, PA, and TJAC; Writing—Original Draft, ECK and TJAC; Writing—Review and Editing, all authors contributed equally.

Conflict of interest

The authors declare that they have no conflict of interest.

References

- Potente M, Mäkinen T (2017) Vascular heterogeneity and specialization in development and disease. *Nat Rev Mol Cell Biol* 18: 477–494
- Adair TH, Montani JP (2010) *Angiogenesis*. San Rafael, CA: Morgan & Claypool Life Sciences
- Davis GE, Stratman AN, Sacharidou A, Koh W (2011) Molecular basis for endothelial lumen formation and tubulogenesis during vasculogenesis and angiogenic sprouting. *Int Rev Cell Mol Biol* 288: 101–165
- Dimmeler S, Haendeler J, Rippmann V, Nehls M, Zeiher AM (1996) Shear stress inhibits apoptosis of human endothelial cells. *FEBS Lett* 399: 71–74
- Gut P, Reischauer S, Stainier DYR, Arnaout R (2017) Little fish, big data: zebrafish as a model for cardiovascular and metabolic disease. *Physiol Rev* 97: 889–938
- Chico TJA, Ingham PW, Crossman DC (2008) Modeling cardiovascular disease in the zebrafish. *Trends Cardiovasc Med* 18: 150–155
- Huisken J, Swoger J, Del Bene F, Wittbrodt J, Stelzer EHK (2004) Optical sectioning deep inside live embryos by selective plane illumination microscopy. *Science* 305: 1007–1009
- Lawson ND, Weinstein BM (2002) In vivo imaging of embryonic vascular development using transgenic zebrafish. *Dev Biol* 248: 307–318
- Paone S, Baxter AA, Hulett MD, Poon IKH (2018) Endothelial cell apoptosis and the role of endothelial cell-derived extracellular vesicles in the progression of atherosclerosis. *Cell Mol Life Sci* 76: 1093–1106
- Colombo M, Raposo G, Théry C (2014) Biogenesis, secretion, and intercellular interactions of exosomes and other extracellular vesicles. *Annu Rev Cell Dev Biol* 30: 255–289
- Zamani P, Fereydouni N, Butler AE, Navashenaq JG, Sahebkar A (2018) The therapeutic and diagnostic role of exosomes in cardiovascular diseases. *Trends Cardiovasc Med* 29: 313–323
- Bernal-Mizrachi L, Jy W, Jimenez JJ, Pastor J, Mauro LM, Horstman LL, de Marchena E, Ahn YS (2003) High levels of circulating endothelial microparticles in patients with acute coronary syndromes. *Am Heart J* 145: 962–970
- Charras GT, Coughlin M, Mitchison TJ, Mahadevan L (2008) Life and times of a cellular bleb. *Biophys J* 94: 1836–1853
- van Lessen M, Shibata-Germanos S, van Impel A, Hawkins TA, Rihel J, Schulte-Merker S (2017) Intracellular uptake of macromolecules by brain lymphatic endothelial cells during zebrafish embryonic development. *Elife* 6: e25932
- Hogan BM, Schulte-Merker S (2017) How to plumb a pisces: understanding vascular development and disease using zebrafish embryos. *Dev Cell* 42: 567–583

16. Agbani EO, van den Bosch MTJ, Brown E, Williams CM, Mattheij NJA, Cosemans JMEM, Collins PW, Heemskerk JWM, Hers I, Poole AW (2015) Coordinated membrane ballooning and procoagulant spreading in human platelets clinical perspective. *Circulation* 132: 1414–1424
17. Gerhardt H, Golding M, Fruttiger M, Ruhrberg C, Lundkvist A, Abramsson A, Jeltsch M, Mitchell C, Alitalo K, Shima D et al (2003) VEGF guides angiogenic sprouting utilizing endothelial tip cell filopodia. *J Cell Biol* 161: 1163–1177
18. Gore AV, Monzo K, Cha YR, Pan W, Weinstein BM (2012) Vascular development in the zebrafish. *Cold Spring Harb Perspect Med* 2: 1–22
19. Siekmann AF, Lawson ND (2007) Notch signalling limits angiogenic cell behaviour in developing zebrafish arteries. *Nature* 445: 781–784
20. Parmalee NL, Kitajewski J (2008) Wnt signaling in angiogenesis. *Curr Drug Targets* 9: 558–564
21. Hogan BM, Bos FL, Bussmann J, Witte M, Chi NC, Duckers HJ, Schulte-Merker S (2009) Ccbe1 is required for embryonic lymphangiogenesis and venous sprouting. *Nat Genet* 41: 396–398
22. Gebala V, Collins R, Geudens I, Phng LK, Gerhardt H (2016) Blood flow drives lumen formation by inverse membrane blebbing during angiogenesis in vivo. *Nat Cell Biol* 18: 443–450
23. Kashiwada T, Fukuhara S, Terai K, Tanaka T, Wakayama Y, Ando K, Nakajima H, Fukui H, Yuge S, Saito Y et al (2015) beta-catenin-dependent transcription is central to Bmp-mediated formation of venous vessels. *Development* 142: 497–509
24. Kwon H-B, Fukuhara S, Asakawa K, Ando K, Kashiwada T, Kawakami K, Hibi M, Kwon Y-G, Kim K-W, Alitalo K et al (2013) The parallel growth of motoneuron axons with the dorsal aorta depends on Vegfc/Vegfr3 signaling in zebrafish. *Development* 140: 4081–4090
25. Sehnert AJ, Huq A, Weinstein BM, Walker C, Fishman M, Stainier DY (2002) Cardiac troponin T is essential in sarcomere assembly and cardiac contractility. *Nat Genet* 31: 106–110
26. Packham IM, Gray C, Heath PR, Hellewell PG, Ingham PW, Crossman DC, Milo M, Chico TJ (2009) Microarray profiling reveals CXCR26a is down-regulated by blood flow in vivo and mediates collateral formation in zebrafish embryos. *Physiol Genomics* 38: 319–327
27. Watson O, Novodvorsky P, Gray C, Rothman AM, Lawrie A, Crossman DC, Haase A, McMahon K, Gering M, Van Eeden FJ et al (2013) Blood flow suppresses vascular Notch signalling via dl14 and is required for angiogenesis in response to hypoxic signalling. *Cardiovasc Res* 100: 252–261
28. Notman R, Noro M, O'Malley B, Anwar J (2006) Molecular basis for dimethylsulfoxide (DMSO) action on lipid membranes. *J Am Chem Soc* 128: 13982–13983
29. Fantin A, Vieira JM, Gestri G, Denti L, Schwarz Q, Prykhodzhiy S, Peri F, Wilson SW, Ruhrberg C (2010) Tissue macrophages act as cellular chaperones for vascular anastomosis downstream of VEGF-mediated endothelial tip cell induction. *Blood* 116: 829–840
30. Tammela T, Zarkada G, Wallgard E, Murtomäki A, Suchting S, Wirzenius M, Waltari M, Hellström M, Schomber T, Peltonen R et al (2008) Blocking VEGFR-3 suppresses angiogenic sprouting and vascular network formation. *Nature* 454: 656–660
31. Ziche M, Morbidelli L, Choudhuri R, Zhang HT, Donnini S, Granger HJ, Bicknell R (1997) Nitric oxide synthase lies downstream from vascular endothelial growth factor-induced but not basic fibroblast growth factor-induced angiogenesis. *J Clin Invest* 99: 2625–2634
32. Kojima H, Nakatsubo N, Kikuchi K, Kawahara S, Kirino Y, Nagoshi H, Hirata Y, Nagano T (1998) Detection and imaging of nitric oxide with novel fluorescent indicators: diaminofluoresceins. *Anal Chem* 70: 2446–2453
33. Kojima H, Urano Y, Kikuchi K, Higuchi T, Hirata Y, Nagano T (1999) Fluorescent indicators for imaging nitric oxide production. *Angew Chem Int Ed Engl* 38: 3209–3212
34. Zhang X, Kim WS, Hatcher N, Potgieter K, Moroz LL, Gillette R, Sweedler JV (2002) Interfering with nitric oxide measurements 4,5-diaminofluorescein reacts with dehydroascorbic acid and ascorbic acid. *J Biol Chem* 277: 48472–48478
35. Haller T, Dietl P, Deetjen P, Völkl H (1996) The lysosomal compartment as intracellular calcium store in MDCK cells: a possible involvement in InsP3-mediated Ca²⁺ release. *Cell Calcium* 19: 157–165
36. Zucker RM, Hunter S, Rogers JM (1998) Confocal laser scanning microscopy of apoptosis in organogenesis-stage mouse embryos. *Cytometry* 33: 348–354
37. Gray C, Packham IM, Wurmser F, Eastley NC, Hellewell PG, Ingham PW, Crossman DC, Chico TJ (2007) Ischemia is not required for arteriogenesis in zebrafish embryos. *Arterioscler Thromb Vasc Biol* 27: 2135–2141
38. Thomas JL, Baker K, Han J, Calvo C, Nurmi H, Eichmann AC, Alitalo K (2013) Interactions between VEGFR and Notch signaling pathways in endothelial and neural cells. *Cell Mol Life Sci* 70: 1779–1792
39. Bentley K, Mariggi G, Gerhardt H, Bates PA (2009) Tipping the balance: robustness of tip cell selection, migration and fusion in angiogenesis. *PLoS Comput Biol* 5: e1000549
40. Vanhollebeke B, Stone OA, Bostaille N, Cho C, Zhou Y, Maquet E, Gauquier A, Cabochette P, Fukuhara S, Mochizuki N et al (2015) Tip cell-specific requirement for an atypical Gpr124- and Reck-dependent Wnt/beta-catenin pathway during brain angiogenesis. *Elife* 4: 1–25
41. Hübner K, Cabochette P, Diéguez-Hurtado R, Wiesner C, Wakayama Y, Grassme KS, Hubert M, Guenther S, Belting HG, Affolter M et al (2018) Wnt/beta-catenin signaling regulates VE-cadherin-mediated anastomosis of brain capillaries by counteracting S1pr1 signaling. *Nat Commun* 9: 4860
42. Huang SM, Mishina YM, Liu S, Cheung A, Stegmeier F, Michaud GA, Charlat O, Waellet E, Zhang Y, Wiessner S et al (2009) Tankyrase inhibition stabilizes axin and antagonizes Wnt signalling. *Nature* 461: 614–620
43. Du J, Wei Y, Liu L, Wang Y, Khairova R, Blumenthal R, Tragon T, Hunsberger JG, Machado-Vieira R, Drevets W et al (2010) A kinesin signaling complex mediates the ability of GSK-3beta to affect mood-associated behaviors. *Proc Natl Acad Sci USA* 107: 11573–11578
44. Dekker RJ, van Soest S, Fontijn RD, Salamanca S, de Groot PG, VanBavel E, Pannekoek H, Horrevoets AJ (2002) Prolonged fluid shear stress induces a distinct set of endothelial cell genes, most specifically lung Krüppel-like factor (KLF2). *Blood* 100: 1689–1698
45. Sacilotto N, Monteiro R, Fritzsche M, Becker PW, Sanchez-Del-Campo L, Liu K, Pinheiro P, Ratnayaka I, Davies B, Goding CR et al (2013) Analysis of Dll4 regulation reveals a combinatorial role for Sox and Notch in arterial development. *Proc Natl Acad Sci USA* 110: 11893–11898
46. Kok FO, Shin M, Ni CW, Gupta A, Grosse AS, van Impel A, Kirchmaier BC, Peterson-Maduro J, Kourkoulis G, Male I et al (2015) Reverse genetic screening reveals poor correlation between Morpholino-induced and mutant phenotypes in zebrafish. *Dev Cell* 32: 97–108
47. Savage AM, Kurasamy S, Chen Y, Jiang Z, Chhabria K, MacDonald RB, Kim HR, Wilson HL, van Eeden FJM, Armesilla AL et al (2019) tmem33 is essential for VEGF-mediated endothelial calcium oscillations and angiogenesis. *Nat Commun* 10: 732
48. Thomas DD (2015) Breathing new life into nitric oxide signaling: A brief overview of the interplay between oxygen and nitric oxide. *Redox Biol* 5: 225–233

49. Durdu S, Iskar M, Revenu C, Schieber N, Kunze A, Bork P, Schwab Y, Gil-mour D (2014) Luminal signalling links cell communication to tissue architecture during organogenesis. *Nature* 515: 120–124
50. Syeda F, Hauton D, Young S, Egginton S (2013) How ubiquitous is endothelial NOS? *Comp Biochem Physiol A Mol Integr Physiol* 166: 207–214
51. Lepiller S, Laurens V, Bouchot A, Herbomel P, Solary E, Chluba J (2007) Imaging of nitric oxide in a living vertebrate using a diamino-fluorescein probe. *Free Radic Biol Med* 43: 619–627
52. Joutel A, Corpechot C, Ducros A, Vahedi K, Chabriat H, Mouton P, Alam-owitch S, Domenga V, Cécillion M, Marechal E et al (1996) Notch3 mutations in CADASIL, a hereditary adult-onset condition causing stroke and dementia. *Nature* 383: 707–710
53. Joutel A, Andreux F, Gaulis S, Domenga V, Cecillon M, Battail N, Piga N, Chapon F, Godfrain C, Tournier-Lasserre E (2000) The ectodomain of the Notch3 receptor accumulates within the cerebrovasculature of CADASIL patients. *J Clin Invest* 105: 597–605
54. Karschnia P, Nishimura S, Louvi A (2019) Cerebrovascular disorders associated with genetic lesions. *Cell Mol Life Sci* 76: 283–300
55. Renz M, Otten C, Faurobert E, Rudolph F, Zhu Y, Boulday G, Duchene J, Mickoleit M, Dietrich AC, Rampacher C et al (2015) Regulation of β 1 integrin-Klf2-mediated angiogenesis by CCM proteins. *Dev Cell* 32: 181–190
56. You C, Sandalcioğlu IE, Dammann P, Felbor U, Sure U, Zhu Y (2013) Loss of CCM3 impairs DLL4-Notch signalling: implication in endothelial angiogenesis and in inherited cerebral cavernous malformations. *J Cell Mol Med* 17: 407–418
57. Westerfield M (1993) *The zebrafish book: a guide for laboratory use of Zebrafish (Brachydanio rerio)*. Eugene, OR: University of Oregon Press
58. Chi NC, Shaw RM, De Val S, Kang G, Jan LY, Black BL, Stainier DY (2008) Foxn4 directly regulates *tbx2b* expression and atrioventricular canal formation. *Genes Dev* 22: 734–739
59. Streisinger G, Walker C, Dower N, Knauber D, Singer F (1981) Production of homozygous diploid zebra fish (*Brachydanio rerio*). *Nature* 291: 293–296
60. White RM, Sessa A, Burke C, Bowman T, LeBlanc J, Ceol C, Bourque C, Dovey M, Goessling W, Burns CE et al (2008) Transparent adult zebrafish as a tool for in vivo transplantation analysis. *Cell Stem Cell* 2: 183–189
61. Traver D, Paw BH, Poss KD, Penberthy WT, Lin S, Zon LI (2003) Transplantation and in vivo imaging of multilineage engraftment in zebrafish bloodless mutants. *Nat Immunol* 4: 1238–1246
62. Blum Y, Belting HG, Ellertsdóttir E, Herwig L, Lüders F, Affolter M (2008) Complex cell rearrangements during intersegmental vessel sprouting and vessel fusion in the zebrafish embryo. *Dev Biol* 316: 312–322
63. Bergmann K, Santoscoy PM, Lygdas K, Nikolaeva Y, MacDonald RB, Cunniffe VT, Nikolaev A (2018) Imaging neuronal activity in the optic tectum of late stage larval zebrafish. *J Dev Biol* 6: 6
64. Ninov N, Borius M, Stainier DYR (2012) Different levels of Notch signaling regulate quiescence, renewal and differentiation in pancreatic endocrine progenitors. *Development* 139: 1557–1567
65. van Impel A, Zhao Z, Hermkens DM, Roukens MG, Fischer JC, Peterson-Maduro J, Duckers H, Ober EA, Ingham PW, Schulte-Merker S (2014) Divergence of zebrafish and mouse lymphatic cell fate specification pathways. *Development* 141: 1228–1238
66. Gray C, Loynes CA, Whyte MK, Crossman DC, Renshaw SA, Chico TJ (2011) Simultaneous intravital imaging of macrophage and neutrophil behaviour during inflammation using a novel transgenic zebrafish. *Thromb Haemost* 105: 811–819
67. Huisken J, Stainier DYR (2007) Even fluorescence excitation by multidirectional selective plane illumination microscopy (mSPIM). *Opt Lett* 32: 2608–2610
68. Schindelin J, Arganda-Carreras I, Frise E, Kaynig V, Longair M, Pietzsch T, Preibisch S, Rueden C, Saalfeld S, Schmid B et al (2012) Fiji - an open source platform for biological image analysis. *Nat Methods* 9: 676–682
69. Preibisch S, Saalfeld S, Tomancak P (2009) Globally optimal stitching of tiled 3D microscopic image acquisitions. *Bioinformatics* 25: 1463–1465
70. Kaufmann A, Mickoleit M, Weber M, Huisken J (2012) Multilayer mounting enables long-term imaging of zebrafish development in a light sheet microscope. *Development* 139: 3242–3247
71. Schmitt CE, Holland MB, Jin SW (2012) Visualizing vascular networks in zebrafish: an introduction to microangiography. *Methods Mol Biol* 843: 59–67
72. Weinstein BM, Stemple DL, Driever W, Fishman MC (1995) Gridlock, a localized heritable vascular patterning defect in the zebrafish. *Nat Med* 1: 1143–1147
73. Le Guen L, Karpanen T, Schulte D, Harris NC, Koltowska K, Roukens G, Bower NI, van Impel A, Stacker SA, Achen MG et al (2014) *Ccbe1* regulates Vegfc-mediated induction of Vegfr3 signaling during embryonic lymphangiogenesis. *Development* 141: 1239–1249
74. Geudens I, Herpers R, Hermans K, Segura I, Ruiz de Almodovar C, Bussmann J, De Smet F, Vandevelde W, Hogan BM, Siekmann A et al (2010) Role of delta-like-4/Notch in the formation and wiring of the lymphatic network in zebrafish. *Arterioscler Thromb Vasc Biol* 30: 1695–1702
75. Quillien A, Moore JC, Shin M, Siekmann AF, Smith T, Pan L, Moens CB, Parsons MJ, Lawson ND (2014) Distinct Notch signaling outputs pattern the developing arterial system. *Development* 141: 1544–1552
76. Morton WM, Ayscough KR, McLaughlin PJ (2000) Latrunculin alters the actin-monomer subunit interface to prevent polymerization. *Nat Cell Biol* 2: 376–378
77. Kovács M, Tóth J, Hetényi C, Málnási-Csizmadia A, Sellers JR (2004) Mechanism of blebbistatin inhibition of myosin II. *J Biol Chem* 279: 35557–35563
78. Nakamura K, Taguchi E, Miura T, Yamamoto A, Takahashi K, Bichat F, Guilbaud N, Hasegawa K, Kubo K, Fujiwara Y et al (2006) KR951, a highly potent inhibitor of vascular endothelial growth factor receptor tyrosine kinases, has antitumor activities and affects functional vascular properties. *Cancer Res* 66: 9134–9142
79. Geling A, Steiner H, Willem M, Bally-Cuif L, Haass C (2002) A gamma-secretase inhibitor blocks Notch signaling in vivo and causes a severe neurogenic phenotype in zebrafish. *EMBO Rep* 3: 688–694